Dispersion of the ordinary refractive indices of smectic liquid crystals in free standing films

R. Jaquet and F. Schneider
Theoretische und Physikalische Chemie, Universität Siegen, 57068 Siegen, Germany
(Received 9 November 2005; revised manuscript received 13 April 2006; published 19 July 2006)

The ordinary refractive indices of some smectic-*A* liquid crystals have been measured by means of interference spectra of free standing films as a function of wavelength and temperature. Numerical data are presented for further use. In the Sm-*C* phase one of the principal indices can be measured. If the three principal indices in the Sm-*C* phase would be known the tilt angle could be measured by means of the interference technique with high precision. Predictions of the refractive index of liquid crystals based on quantum chemical calculations of polarizabilities are presented. Using an expression derived by de Jeu and Bordewijk [J. Chem. Phys. **68**, 109 (1978)] values for the principal refractive indices have been calculated that can be compared with our experimental results.

DOI: 10.1103/PhysRevE.74.011708 PACS number(s): 61.30.−v, 68.15.+e, 78.20.Ci, 33.15.Kr

I. INTRODUCTION

Knowledge of the refractive indices of liquid crystals plays an important role in many experiments and applications [1]. Numerous experimental studies are, therefore, known on this subject [2]. But in most cases the indices are only determined for one wavelength, usually the sodium D line. Many applications and experiments, however, require the dispersion of the indices or the index difference. For smectic liquid crystals used for free standing film experiments no data are available.

We have measured the dispersion of the ordinary index of refraction for some smectic liquid crystals by means of interference spectra of thick free standing smectic films. It is similar to the Talbot technique used by Warenghem *et al.* [3,4] for films aligned between glass plates. Free standing films have the unique property of perfect alignment of the director and constant thickness over large areas. Furthermore, it is very simple to draw films with thicknesses between two and several thousand molecular lengths. A drawback as compared with planar films between glass plates is the perpendicular alignment of the director with respect to the film plane. Therefore only the ordinary refractive index can be measured with the usual light direction perpendicular to the film plane. Talbot and interference spectra yield the full dispersion curve in one experimental run which can be performed in some seconds if an imaging spectrograph is used. Thus it is possible to determine the temperature dependence of the dispersion for several liquid crystals in a reasonable time. The light source and the spectrograph determine the wavelength range of the apparatus. In our setup the wavelengths cover the range from 375 up to 800 nm.

Most of the experiments were performed with liquid crystals in the Sm-*A* phase. In the Sm-*C* phase liquid crystals become biaxial and the indicatrix is tilted with respect to the film normal. The tilt direction can be fixed by applying an electric field in the film plane. Thus two indices can be measured. One of these indices corresponds to a principal refractive index; the other is a combination of two indices. If the principal indices would be known the evaluation of the interference spectra would allow one to determine the tilt angle with high precision. Is it possible to support these measurements by predicting the dispersion behavior using quantum chemical calculations?

In the case of liquid crystals the individual molecules are typically rodlike, and the molecules exhibit an orientational order quantified by the orientational order parameter $S=\frac{1}{2}\langle 3\cos^2\theta-1\rangle$. θ is the angle between the director and the long axes of the molecules. The bracket denotes an average over the molecules in a sufficiently large volume. In smectic phases where the molecules are oriented in layers typical values are $S=0.7$ to 0.8. $S=1.0$ means a perfect orientation. To simulate with classical or *ab initio* molecular dynamics theory [5,6] an ensemble of rodlike molecules on a microscopic level for a given temperature and density is beyond our limits.

Electronic polarizabilities describe the distortion of molecular electron clouds caused by external electric fields (i.e., electromagnetic radiation fields). Within the present work we calculate only the polarizability of one molecule for an optimized conformation and neglect the influence of the environment. Conformational effects are in general not included in the present work. The polarizabilities are used to calculate the indices of refraction with the Lorentz-Lorenz equation and refined methods.

The quality of the electronic polarizabilities depends on the quantum chemical methods and the basis sets [7–9]. The polarizability is the second derivative of the electronic energy with respect to the electric field. It can be calculated (a) by sum-over-states methods [8,10], which involve the determination of all electronic excited states, or (b) more efficiently by means of propagator or response methods [8,11]. In case of higher derivatives (i.e., second derivatives) one needs the calculation of the wave-function response which leads to coupled perturbed equations, e.g., coupled perturbed Hartree-Fock, coupled-perturbed Kohn-Sham, etc. The most simple propagator method with a Hartree-Fock reference is known as the random phase approximation (RPA), which is identical to the time-dependent Hartree-Fock (TD-HF) or coupled Hartree-Fock approach. Equivalent formulations are available with a reference wave function derived from density functional theory. Equations of motion methods used in connection with correlated wave functions, e.g., coupled

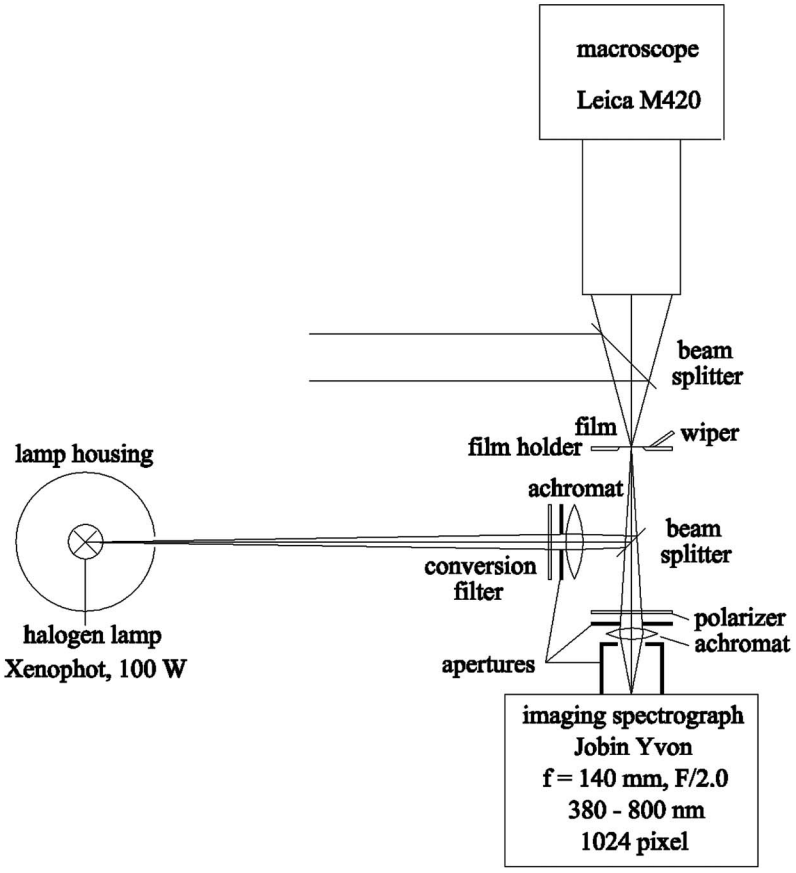

FIG. 1. Schematic diagram of the optical setup. Thermostated housing for the film, windows in the housing, light traps, motor driven micrometer screw for the wiper movement, and macroscope illumination are not shown. The polarizer is only used for the measurement of Sm-*C* films.

cluster methods (CC), are too CPU-demanding for our molecules.

The polarizability depends on the quality of the electronic wave function: Hartree-Fock wave functions lead to reasonable results (polarizabilities are a bit too small), the use of correlated wave functions is too CPU-time consuming. A cheaper alternative way than using correlation methods is to use density functional theory with a functional (e.g., B3LYP), which is known for providing relatively good results accounting for a part of the correlation [12]. It is known for many, but small molecules that DFT(B3LYP) is slightly overestimating and RPA-HF is underestimating polarizabilities [12]. In addition, the quality of polarizability results depends strongly on the quality of the basis set, which has to be "flexible," i.e., additional diffuse functions at least of *s*- and *p*-type are necessary for the heavier elements. Several basis set convergency studies for the static polarizability components, e.g., of benzene [13] and fullerene [13], and comparison with experiment (benzene [14–16], C_{60} [17,18]) are given in the literature.

Because the "liquid crystal" molecules are built from well-known molecular fragments, such as *n*-octane, benzene, biphenyl, etc., we tried to quantify the quality of our results by comparing calculated refractive indices of the molecular fragments with experimental ones.

II. EXPERIMENT

A. Experimental methods

Films were drawn with a wiper across a 14 mm aperture in a film holder (see Fig. 1). The wiper was moved by means of a motor driven micrometer screw. Rapid wiper movements for the generation of thin films were manually performed. Usually aluminum film holders and wipers were used. As the fluorine containing liquid crystal IS1405 decomposed on that surface a polymer holder (Victrex, PEEK) and a glass wiper were used in this case. During the measurements the sample volume was flushed with nitrogen (99.996%).

Film and film holder are surrounded by a thermostated housing with a temperature stability of ±0.01 K. Two inclined glass windows allowed the observation of the film from above and below. Furthermore, additional glass windows were used to maintain the temperature stability at the film and light traps to avoid stray light.

Visual observation of the film during drawing is performed with a macroscope (Leica, M420). Coaxial illumination with a usual microscope illuminator is accomplished by means of a beam splitter made from a 0.15 mm glass plate.

Interference spectra were measured in reflection. The light source is a halogen lamp (Osram, Xenophot, 100 W). First tests with a parallel beam showed that the form of the filament image on the imaging spectrograph depends on the film thickness due to film bending caused by gravity. Therefore the filament was imaged on the film by means of an achromat (f=80 mm). An aperture of 4 mm gives a maximum deviation from normal incidence of 1°. The conversion filter (Linos, TL60) reduces the light intensity at the wavelength of the maximum signal of the imaging spectrograph and transmits the light at short and long wavelengths.

TABLE I. Acronyms, transition temperatures in °C, and sources for the liquid crystals studied. Sources: 1: Synthon GmbH, Wolfen; 2: BDH, Poole; 3: Halle group; 4: G. Heppke, Berlin; and 5: Merck KGaA, Darmstadt.

Liquid crystal	Acronym	Phase sequence	Source
Octyl-cyanobiphenyl	8CB	C 21 Sm-*A* 33.0 N 40.3 I	1
Nonyl-cyanobiphenyl	9CB	C 42 Sm-*A* 47.8 N 49.7 I	2
Dodecyl-cyanobiphenyl	12CB	C 46 Sm-*A* 58.3 I	2
Octyloxy-cyanobiphenyl	8OCB	C 54 Sm-*A* 67.0 N 80.1 I	2
Nitrophenyl-octyloxy-benzoate	NPOB	C 50 Sm-*A* 61.2 N 67.9 I	3
Octyl-[hexyloxyphenyl]-pyrimidine	86OPPY	C 27 Sm-*C* 47.1 Sm-*A* 57.9 N 65.9 I	1
Octyl-[octyloxyphenyl]-pyrimidine	88OPPY	C 34 Sm-*C* 56.3 Sm-*A* 63.2 N 69.3 I	1
Pentylphenyl-octyloxy-thiobenzoate	8OS5	C 58 Sm-*C* 55.9 Sm-*A* 63.0 N 86.0 I	4
See Fig. 2	IS1401	C 32 Sm-*A* 109.2 N 137.1 I	5
See Fig. 2	IS1405	C 29 Sm-*X* 29.6 Sm-*A* 72.9 N 118.5 I	5

The spectra were recorded with an imaging spectrograph (Jobin Yvon, $f=140$ mm, 375–800 nm, 1024 pixel). After calibration with 30 spectral lines between 378 nm (Tl) and 795 nm (Rb) the precision of the wavelength determination of the interference spectra is better than 0.1 nm. 16 bit intensity resolution and averaging of the recordings (20–100 times) resulted in spectra with high signal-to-noise ratios.

A special film holder made from PEEK was used for the alignment of Sm-*C* phases. It contained a rectangular aperture of 8×12 mm and two Ag electrodes at the 12 mm sites. ac voltages up to 1000 V_{rms} at 1000 Hz were applied to the electrodes. Dispersion measurements were only performed if the film was free from disclinations.

Refractive indices at 589 nm were determined with a calibrated Abbé refractometer using a sodium spectral lamp. The variation of the refractive index of the measuring prism with temperature was taken into account $(-0.68\times10^{-5}(t-20)$, t in °C [19]). The prism surfaces were cleaned by antiparallel rubbing with cleaning tissues (kimwipes) wetted with acetone. Then a cleaning tissue was wetted with a solution of 0.3% lecithin in toluene and drawn over the prisms giving a homeotropic alignment. The problematic determination of the probe temperature was accomplished by means of a thermocoax thermoelement with a diameter of 0.5 mm in the water outlet of the measuring prism. The thermoelement and the temperature measuring device for the film housing were calibrated with a thermometer with mK precision (Paar, MKT25). The upper temperature limit for the measurements of 80 °C was determined by the Abbé refractometer.

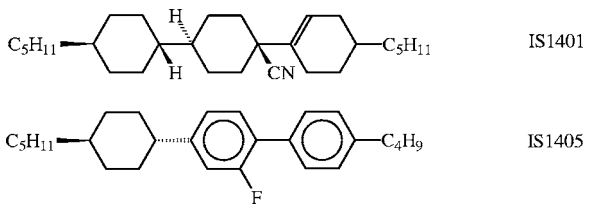

FIG. 2. Molecular structures.

Table I shows the liquid crystals studied (see Fig. 2). IS1405 was recrystallized from ethanol at −20 °C. All other liquid crystals were used without further purification. The melting points were determined with a DSC from Mettler-Toledo. All other transition temperatures were determined with a polarizing microscope equipped with a hot stage.

B. Evaluation of measurements

The reflection spectra recorded by the imaging spectrograph have to be calibrated with respect to the intensities. The calibration curve $I_c(\lambda)$ strongly depends on position, orientation, and bending of the reflecting surface. The simplest and most precise calibration method is to measure the reflected intensity of a thin film itself.

For normal incidence the reflected intensity I for a film with thickness D, ordinary refractive index n_o, and wavelength λ is

$$\frac{I}{I_0}=\frac{4R\sin^2(\delta/2)}{(1-R)^2+4R\sin^2(\delta/2)}, \tag{1}$$

where $\delta=4\pi n_oD/\lambda$, $R=(n_o-1)^2/(n_o+1)^2$ and λ is the wavelength. For thin films this equation can be expanded in δ to give

$$\frac{I}{I_0}=\pi^2(n_o^2-1)^2\frac{D^2}{\lambda^2}+O(\lambda^{-4}). \tag{2}$$

Equation (2) predicts a simple $1/\lambda^2$ dependence on the wavelength. Furthermore, the film thickness must not be known for the calibration with thin films if only relative intensities are to be determined.

Nevertheless, we have used Eq. (1) for the calibration. This allows us to use films with thicknesses for which Eq. (2) leads to errors. The calibration equation is

$$I_{norm}=I_{raw}\frac{\left[\dfrac{4R\sin^2(\delta/2)}{(1-R)^2+4R\sin^2(\delta/2)}\right]_{cal}}{I_{cal}}. \tag{3}$$

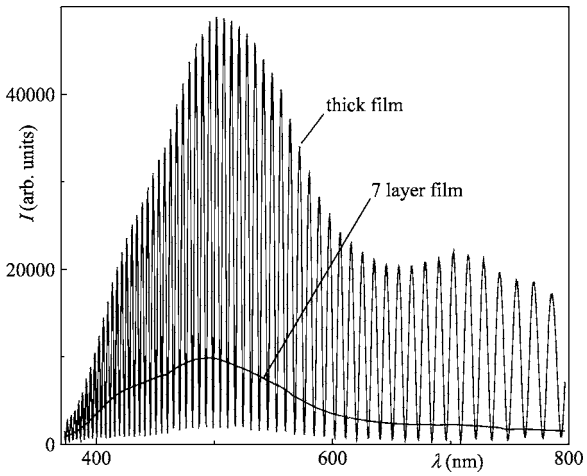

FIG. 3. Raw interference spectra of a thick and a thin film of 8CB at 21.85 °C in the smectic-*A* phase.

The index cal refers to the thin film: I_{cal} is the measured intensity and $[\ldots]_{cal}$ is the result predicted by Eq. (1).

The film thickness

$$D = Nd \tag{4}$$

was determined from the thickness d of the smectic layer which is usually known from x-ray investigations and the small integer layer number N. Wrong layer numbers lead to wrong maximum intensities of the interference spectra of thick films. It is known that there is a difference in the thicknesses of the inner and outer layers of a film due to the enhanced ordering of the outer layers. This difference has only a minor influence on the calibration as for thin films with few layers the form of the calibration curve will not change [see Eq. (2)].

Figure 3 shows an example for the raw data for a thick film of 8CB and a thin film used for the calibration. Calibration leads to the normalized spectrum shown in Fig. 4. The

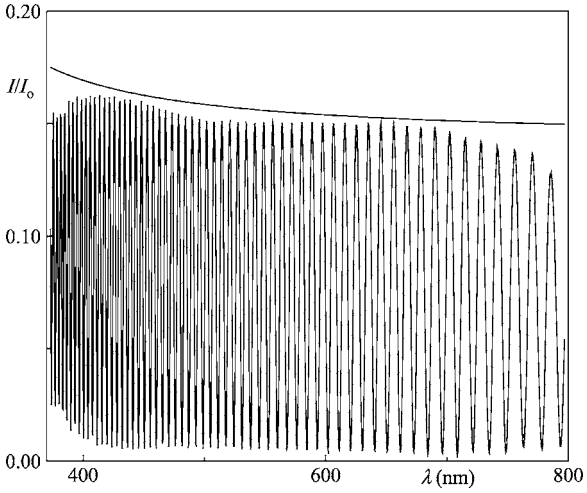

FIG. 4. Normalized interference spectrum of a thick film of 8CB at 21.85 °C and calculated amplitude. I_0 is the incident intensity.

smooth curve shows the amplitudes of the reflected intensities.

$$\frac{I}{I_0} = \frac{4R}{(1-R)^2 + 4R} = \frac{[n(\lambda)^2 - 1]^2}{[n(\lambda)^2 + 1]^2}. \tag{5}$$

The measured maximum values are somewhat smaller than the values according to this equation. At the shortest wavelengths this is surely due to the missing resolution of the spectrograph. This also leads to the nonvanishing intensities at the minima. The reduced intensities of the maxima at the longest wavelengths could not be explained. It may be that this is caused by the bending of the thick films and the nonperfect achromatic imaging of the light source on the spectrograph. The errors of the calibration procedure only have a minor influence on the evaluation of the refractive indices because they are determined from the positions of the minima on the λ axis of the intensity curve.

The minima of Eq. (1) occur at

$$2nD = k\lambda. \tag{6}$$

If the film thickness D and the interference order k are known, the dispersion of the refractive index can be determined very simply. k increases by one for every minimum at shorter wavelengths beginning with $k=k_0$ at the long wavelengths end ($\approx$800 nm) of the spectrum. k_0 can be determined from the wavelengths (λ_0, λ_-) of two adjacent minima at this end of the spectrum.

$$k_0 = \lambda_-/(\lambda_0 - \lambda_-). \tag{7}$$

This equation gives interference orders which are too high due to the dispersion. Taking into account a mean linear dispersion $(\partial n/\partial\lambda)_0 = -3.5 \times 10^{-5}$ nm^{-1} gives

$$k_0 = \frac{\lambda_-}{(\lambda_0 - \lambda_-)\left[1 - \frac{\lambda_0}{n_0}\left(\frac{\partial n}{\partial \lambda}\right)_0\right]}. \tag{8}$$

The calculated k_0 values now show maximum deviations of ± 1 from the correct values. The correct values can be determined from measurements on two films with different thicknesses (see Fig. 5). If films with larger thickness differences are used, stronger deviations in the curves result. Usually it is sufficient to calculate dispersion curves for a film with k_0 given by Eq. (8) and with the two neighboring values $k_0 \pm 1$. For film thicknesses of 10–15 μm used in our experiments the following behavior is observed: That k value which exceeds the correct value by one gives a refractive index curve with a constant or even with a positive dispersion for long wavelengths.

The second unknown quantity in Eq. (6) is the film thickness D. A procedure for the determination of the film thicknesses was introduced for the calibration of the measured intensities [see Eq. (4)]. This procedure can only be used for thin films and not for the thick films used for the dispersion measurements. A procedure for the determination of D that was proposed in an earlier study [20] also cannot be applied for the thick films used in this study. In the present work we have measured the ordinary refractive index at 589 nm with

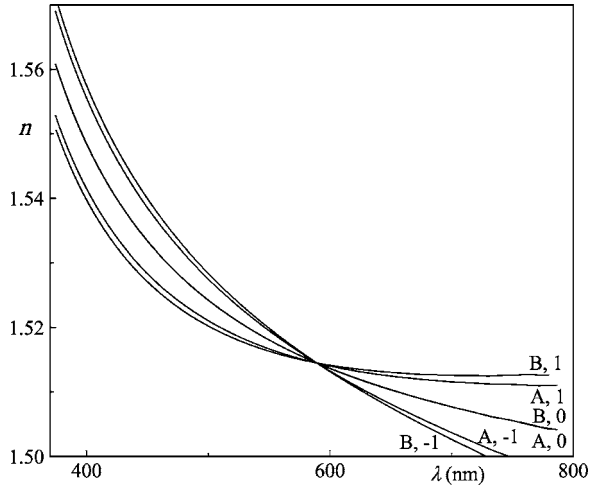

FIG. 5. Calculated dispersion curves for two 8CB films with different thicknesses: A: 14.4, B: 11.4 μm. The second parameter at the curves gives the deviation Δk in the interference order from the value calculated with Eq. (8). The two curves for $\Delta k=0$ are not distinguishable within the resolution of the diagram.

an Abbé refractometer and calculated D with Eq. (6) using the known k value. Due to this procedure the curves in Figs. 5 and 6 intersect at 589 nm.

Errors with this method of measurement are only caused by the error of the starting value at 589 nm, the deviation of the light beam from normal incidence, and the precision of the determination of the minima in the intensity curve. Figure 6 shows the deviations in the refractive index for measurements with films of different thicknesses. The deviations are calculated as follows. The dispersion for one of the measurements ($D=11.7$ μm) was fitted with the Hartmann equation extended by a λ^2-term

$$n = A + \frac{B}{\lambda - C} + D\lambda^2 \tag{9}$$

and the differences to this fit were plotted in Fig. 6. The deviations are generally smaller than 0.0001 which is smaller

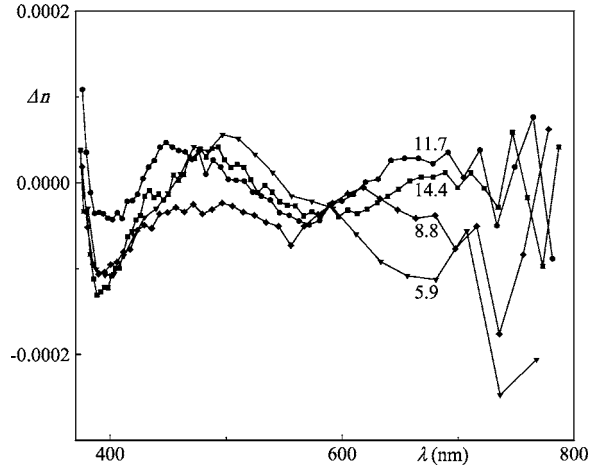

FIG. 6. Deviation of the dispersion curves from the Hartmann equation (9). 8CB films with different thicknesses D: 14.4, 11.7, 8.8, and 5.9 μm.

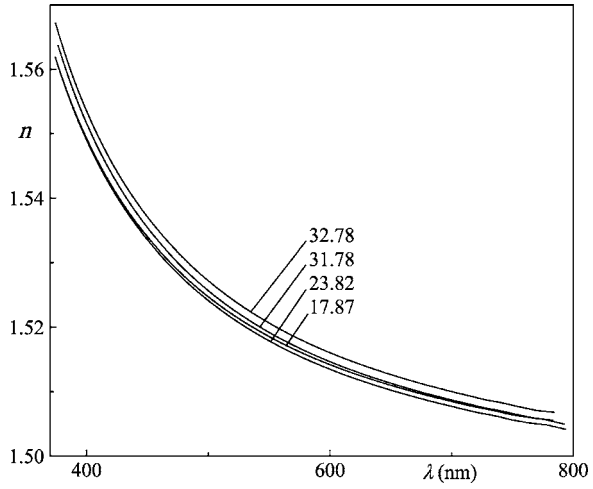

FIG. 7. Dispersion curves of 8CB at different temperatures in °C.

than the error of the reference value at 589 nm. Due to the broader minima and the amplitude variation at longer wavelengths the deviations become stronger at long wavelengths. Thicker films give more precise results. However, an upper limit for the thickness results from the fact that our algorithm for the determination of the minima needs at least six data points between the neighboring maxima and the number of these data points decreases with the film thickness. This leads to the upper limit of about $D=25$ μm for the film thickness with our imaging spectrograph.

C. Experimental results

1. Sm-*A phases*

The dispersion of 8CB is shown in Fig. 7 for some temperatures. Besides the shortest wavelengths the ordinary refractive index shows the usual behavior as a function of temperature (Fig. 8). At low temperatures it decreases with increasing temperature due to the change of the density. At high temperatures it increases with increasing temperature.

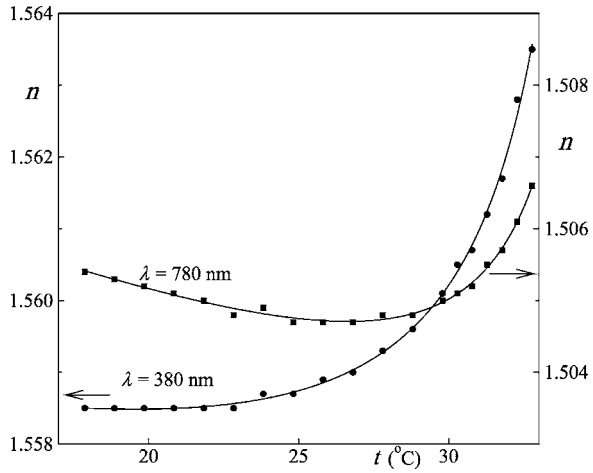

FIG. 8. Index of refraction of 8CB as a function of temperature at $\lambda=380$ and 780 nm.

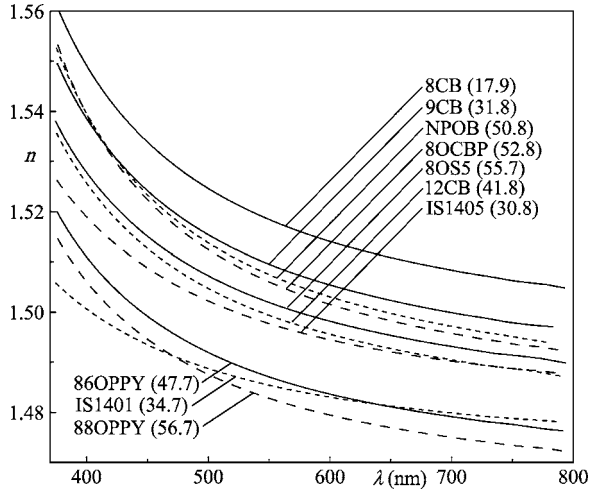

FIG. 9. Dispersion curves of the liquid crystals studied at the lowest temperatures of measurement shown in parentheses in °C.

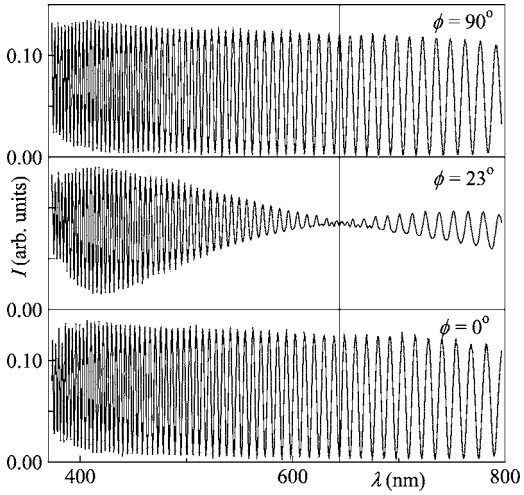

FIG. 10. Interference spectra of 86OPPY in the Sm-*C* phase at 30 °C. ϕ is the angle between tilt and polarization direction.

This is caused by the decrease of the orientational order parameter which leads to an averaging of the polarizabilities [see Eqs. (13) and (14)]. Nearly all liquid crystals studied show the following peculiar effect (see Fig. 8) at short wavelengths. At 380 nm the index of refraction exhibits a constant value and does not show the usual increase of the index at low temperatures due to the change of the density. Surely this effect is limited to a small temperature area. At lower temperatures which are not accessible due to crystallization of the sample the increase of the index of refraction will begin. This effect is probably caused by the strong increase of the birefringence $\Delta n = n_e - n_o$ for shorter wavelengths [21]. This leads to the enhanced rise in the neighborhood of the transition to the nematic phase.

The comparison of the dispersion curves for the liquid crystals (see Fig. 9) was performed at the lowest temperatures of measurement which was some degrees below the melting point or at the transition to the Sm-*C* phase. The influence of the order parameter at this temperature is expected to be small.

The dispersion curves for the alkyl-cyano-biphenyls are shifted against one another while having the same form. This is due to the "dilution" of the aromatic cores by the alkyl chains with their small polarizability. The dilution effect increases with the alkyl chain length. The corresponding alkyloxy (8OCB) compound shows a stronger increase of the refractive index at short wavelengths due to an absorption maximum at 291 nm in cyclohexane as compared with 272 nm for 8CB [22]. The smallest dispersion is shown by IS1401 which exhibits only one isolated double bond. A more detailed discussion is presented in the theory section III B.

The refractive indices of all liquid crystals studied are listed in Table V in Appendix A.

2. Sm-*C* phases

The evaluation of interference spectra in Sm-*C* phases is considerably more complicated. Figure 10 shows an example for 86OPPY in the Sm-*C* phase. The director is inclined with respect to the film normal and the interference spectrum depends on the polarization direction. The interference spectrum for $\phi = 23°$ is a superposition of the spectra at 0° and 90°. The smallest amplitude of the beat is not observed at $\phi = 45°$ as the interference spectra for 0° and 90° show different intensities due to the beam splitter. This is taken into account in the calibration procedure for the upper and lower spectrum of Fig. 10. The intensity for the 90° spectrum is 5.62 times higher than that of the 0° spectrum. This ratio leads to the smallest amplitude at $\phi = 23°$.

At approximately 420 nm the two interference spectra are in phase and the beginning of the amplitude reduction due to the next minimum is observed.

A schematic indicatrix of an Sm-*C* phase with the three principal refractive indices n_α, n_β, and n_γ is shown in Fig. 11. In the Sm-*C* phase the γ axis is inclined by the tilt angle Θ with respect to the film normal which is parallel to the

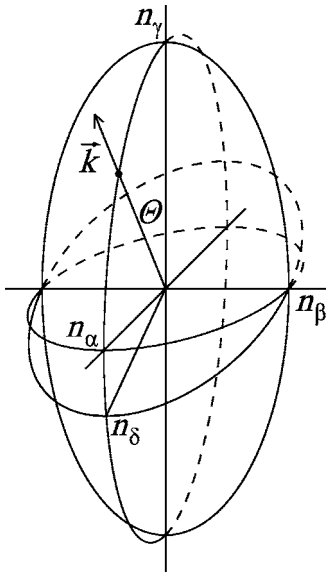

FIG. 11. Indicatrix of an Sm-*C* phase. n_α, n_β, and n_γ: principal refractive indices; Θ: tilt angle; and $\vec{k}$: wave normal, film normal.

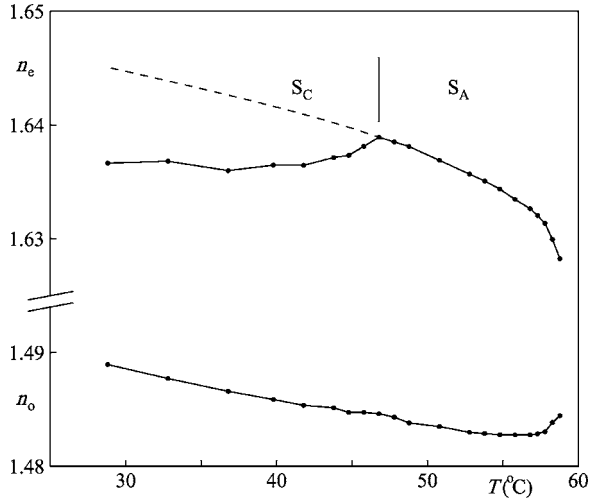

FIG. 12. Refractive indices of 86OPPY at 589 nm as a function of temperature. The dashed line is a manually drawn continuation of the extraordinary index in the Sm-*A* phase.

wave normal $\vec{k}$. The indices which can be observed in the experiment are the semiaxes of the ellipse which is obtained by cutting the wave front through the origin with the indicatrix. These indices are n_β and n_δ where

$$\frac{1}{n_\delta^2} = \frac{\cos^2\Theta}{n_\alpha^2} + \frac{\sin^2\Theta}{n_\gamma^2}. \tag{10}$$

The polarization directions are parallel to the principal axes of the ellipse. The interference experiment with $\phi=0°$ corresponds to n_δ and $\phi=90°$ to n_β.

If the principal refractive indices would be known the measurement of n_δ with the interference experiment would give a very precise measurement of the tilt angle. Unfortunately, we did not succeed in measuring the principal indices of the pyrimidines in the Abbé refractometer with a planar director alignment as described by Lockhart *et al.* [23,24]. Our surface preparation (see Sec. II A) of the prisms gives a homeotropic alignment in the Sm-*A* phase. In the Sm-*C* phase we observe a sharp shadow line for the light polarized perpendicular to the rubbing direction and the prism normal (vertical polarization). The temperature dependence of the corresponding refractive index is a continuation of the ordinary index in the Sm-*A* phase. For the horizontal polarization we observe sometimes near the transition from the Sm-*A* phase two shadow lines. At lower temperatures we always find one very diffuse shadow line which is not a continuation of the extraordinary index in the Sm-*A* phase (see Fig. 12). These observations suggest that the tilt direction is parallel to the rubbing direction, but the tilt lies somewhere between 0° and the tilt angle. Thus we are only able to measure n_β exactly.

However, the tilt angle can be estimated as follows. n_γ is determined from the continuation of the extraordinary index in the Sm-*A* phase: $n_\gamma=1.645$ at 30 °C. The difference between n_α and n_β is usually very small ($\approx 10^{-3}$) [23,24]. Therefore we use the measured n_β value for n_α ($n_\alpha=1.4885$). The thickness of the film at 30 °C is determined from the interference experiment at $\phi=90°$ and the refractometer value for n_β ($D=13.763$ nm). The refractive index n_δ at 589 nm for the evaluation of the interference spectrum at $\phi=0°$ is now varied such that the calculated film thickness agrees with the known value. The resulting value is $n_\delta=1.5003$. Finally the tilt angle is determined by means of Eq. (10). The value $\Theta=17.1°$ agrees well with the tilt angle of 17° for 86OPPY as determined by Koden and Anabuki [25] at 20 °C.

III. QUANTUM CHEMICAL CALCULATIONS

The quantum mechanical methods and basis sets needed for the calculation of frequency dependent polarizabilities are described in Appendix B. We have mostly used time-dependent Hartree-Fock (TD-HF) and time-dependent density functional theory (TD-DFT) using the B3LYP functional, which is a compromise between accuracy and efficiency.

In recent years static and dynamic polarizabilities of a series of small molecules have been calculated using HF, DFT [12], and CC [26] methods. For larger molecules semiempirical methods have been favored (polycyclic aromatic molecules: [27], and C_{60}: [28,29]); for the accurate calculation of the polarization tensor components semiempirical methods seem to be inadequate. Van Caillie and Amos [12] have investigated in detail static and dynamical polarizabilities using SCF (self-consistent field), DFT (LDA, B3LYP), and CCSDLR [CCSD: (coupled cluster with singles and doubles), LR: (linear response)] for a series of smaller molecules. Their calculations showed that a reasonable degree of accuracy is obtained if DFT in conjunction with a hybrid functional such as B3LYP is used.

At the beginning of our studies we could perform only RPA calculations for $\alpha(\omega)$ on the SCF level and used calculated static polarizabilities on the B3LYP level (6-31++G* basis set) to extrapolate $\alpha(\omega)$ to the "correct" basis set limit including correlation effects (DFT). Later on we were able to calculate time-dependent polarizabilities on the DFT level. Similar calculations of $\alpha(\omega)$ for liquid crystal molecules of the size described in the present work have not been performed before.

Basis sets often used for high quality calculations of polarizabilities of small molecules, e.g., Sadlej's polarized basis set [30], are too demanding with respect to CPU and memory requirements in the present work. These basis sets have already been used for smaller molecules in order to verify the usefulness of the extrapolation procedure.

A. The refractive index

For a given average molecular polarizability α the refractive index n of a liquid can be computed using the Lorentz-Lorenz formula [31,32]

$$\frac{n^2-1}{n^2+2} = \frac{4}{3}\pi N\alpha, \quad \alpha = (\alpha_{uu}+\alpha_{vv}+\alpha_{ww})/3, \tag{11}$$

where N represents the number density of molecules and u, v, and w are the principle axes of the tensor $\underline{\underline{\alpha}}$. $\underline{\underline{\alpha}}$ and n are

frequency dependent properties (dispersion relation). The Lorentz-Lorenz formula does not have a firm theoretical basis for liquids of anisotropic molecules, but, nevertheless, it is widely used for the determination of the average polarizability of anisotropic molecules. A similar equation is used for the calculation of dielectric constants ϵ (equation of Clausius and Mosotti) using $n^2=\epsilon$.

A semiempirical formula connecting the components of the microscopic polarizabilities α_{ii} to the macroscopic refractive indices n_i of a crystal has been presented by Vuks [33]:

$$\frac{n_u^2-1}{n^2+2}=\frac{4}{3}\pi N\alpha_{uu} \tag{12}$$

and similar equations for α_{vv} and α_{ww}. n^2 is the mean value $n^2=(n_u^2+n_v^2+n_w^2)/3$.

In this equation the local field effect has been assumed to be isotropic. In order to apply this equation to liquid crystals the anisotropic local field and the nonperfect alignment has to be taken into account. De Jeu and Bordewijk [34,35] investigated refractive indices and internal fields in nematic azoxybenzenes. They suggested an expression for the dielectric constants $\epsilon_\parallel$ and $\epsilon_\perp$ that takes into account the influence of the macroscopic order parameter S and the anisotropic local field:

$$\epsilon_\parallel=1+\frac{4}{3}\pi N\left[\frac{\alpha_l(2S+1)}{1-4\pi N\alpha_l\Omega_l}+\frac{\alpha_t(2-2S)}{1-4\pi N\alpha_t\Omega_t}\right], \tag{13}$$

$$\epsilon_\perp=1+\frac{4}{3}\pi N\left[\frac{\alpha_l(1-S)}{1-4\pi N\alpha_l\Omega_l}+\frac{\alpha_t(2+S)}{1-4\pi N\alpha_t\Omega_t}\right]. \tag{14}$$

The indices l and t define for a prolate molecule the longitudinal and transversal axes, respectively. In this system of coordinates the polarizability tensor has a nearly diagonal form. The values we are using in the calculation belong to the diagonalized α tensor whose axes are slightly tilted with respect to the original axes. The resulting components α_{uu}, α_{vv}, and α_{ww} do increase by a few percent. α_l and α_t are the principal values for a prolate spheroid:

$$\alpha_l=\alpha_{uu},\quad \alpha_t=\frac{1}{2}(\alpha_{vv}+\alpha_{ww}). \tag{15}$$

The principal values of the so-called shape or depolarizing factors Ω_l and Ω_t take into account "volume" contributions of the spheroid. The shape factors depend on the axial ratio L/T for a spheroidal molecule with principal axes L (long axis) and T and are given by

$$\Omega_l=1-W^2+\frac{1}{2}W(W^2-1)\ln[\,(W+1)/W-1)],$$

$$\Omega_t=\frac{1}{2}(1-\Omega_l),$$

$$W^2=L^2/(L^2-T^2),\quad T=\frac{1}{2}(T_v+T_w). \tag{16}$$

The sizes L and T of the prolate molecules have been calculated within G98 and are presented in Table III.

We use Eqs. (13) and (14) with $\epsilon_\parallel=n_e^2$ and $\epsilon_\perp=n_o^2$ to calculate the ordinary (n_o) and extraordinary (n_e) refractive index from the computed polarizabilities. The polarizabilities as well as the refractive indices depend on frequency. The representation

$$\alpha(\omega)=\alpha(0)+S(-4)\times\omega^2+S(-6)\times\omega^4+\cdots \tag{17}$$

can be used in which the quadratic regression constants give the $S(-4)$ Cauchy coefficients, also known as dipole oscillator strength sum. These values are experimentally well-known for small molecules (see references in Ref. [12]), but not for our "liquid crystal molecules." A comparison of the dispersion of the refractive index between experiment and *ab initio* calculations (see, e.g., Fig. [16]) shows that although there is a small absolute deviation, the frequency dependency is in nearly perfect agreement. We also expect that the calculated frequency dependence of the polarizability [i.e., the $S(-4)$ term in the expansion of Eq. (17)] is described rather accurately using the data for frequency dependent polarizabilities presented in the next section.

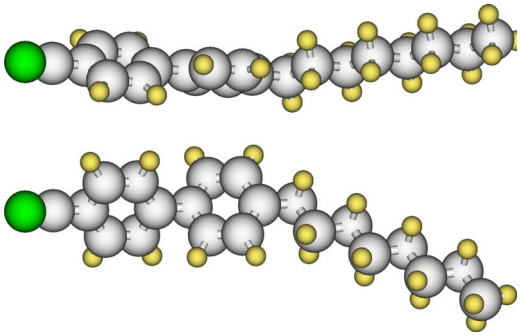

FIG. 13. (Color online) 8CB: two different views of the optimized structure (B3LYP/6-31G*).

B. Theoretical results

For all molecules presented in Table I structures have been optimized using DFT (B3LYP functional, 6-31G* basis set). The geometries for the lowest electronic energies of 8CB and 88OPPY are presented in Figs. 13 and 14. The

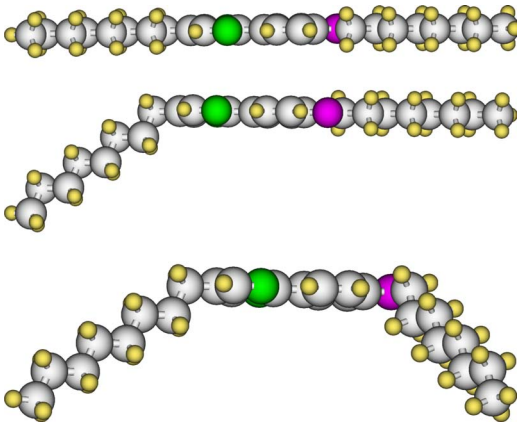

FIG. 14. (Color online) 88OPPY optimized with B3LYP/6-31G* (with relative stability E_{rel}): top: 88OPPY(1), planar, E_{rel}=5.65 kJ/mol; middle: 88OPPY(2), "nearly" planar, E_{rel}=0 kJ/mol; and bottom: 88OPPY(3), nonplanar, E_{rel}=5.36 kJ/mol.

TABLE II. Frequency dependent polarizabilities α in a.u. calculated with random phase approximation (RPA-HF/4-31Gex).

Molecules λ (nm)		8CB	9CB	12CB	8OCB	NPOB	86OPPY	88OPPY(1)	8OS5	IS1401	IS1405
400	α_{uu}	446.49	463.63	509.64	463.20	456.15	499.92	533.61	530.13	386.39	506.62
	α_{vv}	227.51	236.91	271.06	229.32	254.81	282.33	303.60	305.23	251.34	275.28
	α_{ww}	166.86	176.06	204.87	166.42	178.52	203.72	222.91	246.03	265.04	231.46
500		416.52	433.26	478.57	431.35	429.97	470.19	502.96	502.68	379.11	480.53
		221.63	230.88	264.38	223.35	247.88	275.85	296.82	298.34	248.23	269.17
		163.81	172.88	201.24	163.40	175.24	200.41	219.32	241.37	261.25	227.50
600		403.25	419.78	464.70	417.36	417.99	456.97	489.29	489.84	375.31	468.41
		218.67	227.85	261.01	220.36	244.44	272.58	293.38	294.83	246.57	266.06
		162.24	171.23	199.37	161.85	173.56	198.69	217.45	238.97	259.26	225.44
700		396.01	412.42	457.10	409.75	411.36	449.73	481.80	482.66	373.07	461.65
		216.96	226.09	259.06	218.63	242.46	270.68	291.38	292.79	245.59	264.25
		161.32	170.27	198.26	160.94	172.58	197.68	216.36	237.56	258.09	224.23
800		391.57	407.90	452.44	405.09	407.27	445.29	477.19	478.20	371.63	457.46
		215.88	224.98	257.82	217.54	241.21	269.48	290.11	291.49	244.96	263.11
		160.73	169.65	197.56	160.35	171.95	197.04	215.65	236.66	257.33	223.45
∞		378.29	394.38	438.41	391.21	394.91	431.96	463.36	464.61	367.04	444.72
		212.48	221.49	253.92	214.11	237.31	265.68	286.11	287.39	242.92	259.48
		158.86	167.68	195.32	158.50	169.96	194.98	213.41	233.81	254.92	220.98

energetically most stable forms are nearly rodlike. The perfect linear and planar structures lead to higher energies due to the low flexibility of the bond angles between the elements C, N, O, S, etc. Some molecular species prefer to arrange in an alternating way ("dimer"-like structure), e.g., 8CB [36]. We found mostly one energetically stable structure with nearly linear and planar geometry. In the case of 88OPPY (see Fig. 14) the three different structures deviate only by 5.36 and 5.65 kJ/mol from the most stable one, which is not the planar form. Calculations for the three individual conformers have shown that the polarizabilities are comparable.

To our knowledge there are no *ab initio* calculations for the static and frequency dependent polarizabilities of the "liquid crystal molecules" investigated in the present work. The application of linear response theory is sufficient for the wavelength range from 400 to 800 nm because the absorption maxima are lying at much shorter wavelengths. The absorption spectra in cyclohexane show maxima at $\lambda=272$ nm for 8CB and 291 nm for 8OCB [22]. For a MNDO calculation the results are: 8CB: 273 nm; 8OCBP: 280 nm; and NPOB: 296 nm.

To compare with semiempirical calculations is of minor importance, because only semiempirical methods with special parametrizations for spectroscopic properties [37] lead to acceptable average polarizabilities; the individual principal values and anisotropies are far off from being reasonable. We found that using semiempirical methods, especially the polarizability perpendicular to the molecular plane of an aromatic system, deviates strongly from experimental values or *ab initio* calculations. The static polarizabilities calculated with DFT are presented in Table III. In addition, the size of the molecules is given in this table, where the value for T in Eq. (16) is an average of the two smaller principal axis lengths. α_t is the average value of the two smaller components of the polarizability tensor (see Tables II–IV).

Table II shows frequency dependent polarizabilities calculated from 400 nm to the long wavelengths limit (i.e., static) regime. The basis set 4-31Gex is of a size we at most could manage to calculate polarizabilities. The static polarizabilities in Table II (RPA-HF/4-31Gex) can be compared with values in Table III (DFT-B3LYP/6-31++G*) showing an increase of the polarizability. For IS1401 one can see a strong increase with changing the method from RPA-HF to TD-DFT and increasing the basis set; the structure of IS1401 (with three cyclo-hexane groups) deviates strongest from the other molecules.

Table IV summarizes the results for static polarizabilities of the monomer and dimer form of 8CB. It is known [36] that 8CB molecules are packed in a dimerlike structure which might have an influence on the polarizability. Two different structures are compared: geometry taken from x-ray measurements [38] and optimized structures (monomer and dimer). The optimized structure has a larger α_l, whereas for the crystal structures larger values for α_t are found. The contributions in the dimer are slightly smaller for α_l and larger for α_t than two contributions of one monomer $(\Delta\alpha_l, \Delta\alpha_{t_1}, \Delta\alpha_{t_2}: -4\%, 0\%, +2\%)$, if this is based on crystal structures. A similar result is found if the comparison is based on individually optimized structures $(-4\%, -4\%, +7\%)$. In summary, for the optimized structures the polarizabilities in the monomer are larger for α_l and α_{t_1}, but smaller for α_{t_2} than in the dimer. The monomer data using 6-31++G* have been used later to calculate refractive indices. The absolute change in the components of the polarizabilities (monomer versus dimer) is not significant enough to

TABLE III. Static polarizabilities α in a.u. calculated with DFT (B3LYP/6-31++G*), deviations in percent with respect to RPA-HF/4-31Gex ($\Delta\alpha_l$,$\Delta\alpha_t$), and principal axes lengths L, T_v, and T_w in Å for the prolate spheroidal form of the molecules.

Molecules	8CB	9CB	12CB	8OCB	NPOB	86OPPY	88OPPY(1)	8OS5	IS1401	IS1405
α_{uu}	428.57	444.96	490.85	454.09	470.95	479.67	534.71	536.19	446.58	501.35
α_{vv}	221.62	225.05	254.85	224.05	247.67	274.10	302.61	304.84	284.74	272.10
α_{ww}	164.82	184.83	220.91	165.40	178.11	230.32	222.89	247.39	291.95	232.82
$\Delta\alpha_l$	13.29	12.83	11.96	16.07	19.26	11.05	15.40	15.41	21.67	12.73
$\Delta\alpha_t$	4.07	5.32	5.90	4.52	4.54	9.50	5.20	5.95	15.84	5.09
L	19.8796	20.61485	24.17304	21.00226	22.65153	21.81683	27.54812	24.33481	24.27405	22.88647
T_v	5.4217	5.34541	5.96200	5.30731	4.93417	8.68098	7.33062	8.63557	6.50861	5.78693
T_w	3.1387	4.35835	4.49196	2.60350	3.05530	5.37171	2.68438	4.77171	5.67316	5.05415

cause a dramatic influence on the refractive index compared to experiment. The changes are within the range of errors we have to assume for our *ab initio* calculations.

The frequency dependent polarizabilities of 8CB are presented in Fig. 15 for different basis sets. Obviously, the dispersion behavior is similar, but the absolute value depends on the quality of the basis set. The polarizabilities for the low-frequency limit [using TD-DFT(B3LYP)] have also been calculated with the largest basis set (6-31++G*), so that the dispersion curves could be shifted to this reference value.

In Figs. 16 (8CB) and 17 [88OPPY(1)] experimental and two theoretical results of the frequency dependence of the refractive index are presented. Using the originally computed RPA-polarizabilities presented in Table II leads to dispersion curves for fully ordered molecules if the Vuks-equation is used. Contributions due to electron correlation are missing because the RPA-values are based on Hartree-Fock theory. Van Caillie and Amos [12] have shown for a series of small molecules that polarizabilities calculated on the level of density functional theory (with the B3LYP functional) are approximating experimental polarizabilities and accurate theoretical polarizabilities, i.e., including electron correlation, fairly well.

The two theoretical results in Figs. 16 and 17 are calculated in the following way.

(a) We use the Vuks-equation 12 (RPA-HF/4-31Gex), in which it is implicitly assumed that the order parameter S is one.

(b) We use the static polarizabilities calculated on the DFT-B3LYP/6-31++G* level (see Table III) and scale linearly the frequency dependent polarizabilities given in Table II. These values are taken as input for Eqs. (13) and (14). The order parameter is assumed to be $S=0.7$. The order parameter values for 8CB [41] deviate strongly from each other. The mean value is 0.7. For the other molecules we also use 0.7 due to the lack of measurements.

In case of 8CB the scaling leads to an increase of α_l by 13% and for α_t by 4%, which results in a case of the Vuks-equations to an increase of n_e-1 by 14% [$n_e(\lambda=\infty)$: 1.77343 (RPA/4-31Gex), 1.88004 (B3LYP/6-31++G*)] and of n_o-1 by 7% [$n_o(\lambda=\infty)$: 1.43277 (RPA/4-31Gex), 1.46380 (B3LYP/6-31++G*)]. If one uses the de Jeu-Bordewijk expression (including scaling) the n_e-1 values for $S=1.0$ reduce with respect to the values using the Vuks-equations by 29% [see Eqs. (13) and (14) and $n_{e,o}(\lambda=\infty)$: 1.68405, 1.46345], whereas n_o remains approximately constant. For $S=0.7$ n_e-1 reduces further by 6%, whereas n_o-1 increases by 5%. Similar results are presented in Fig. 17 for 88OPPY, where we considered only the structure related to 88OPPY(1) (see Fig. 14, top). In Figs. 16 and 17 we can

TABLE IV. 8CB: Monomer and dimer static polarizabilities in a.u. calculated with DFT (B3LYP) using the basis set 6-31++G*. The structure of the molecule has been optimized (opt) or taken directly from x-ray measurements [38] (cryst).

		α_{uu}	α_{vv}	α_{ww}
Monomer				
8CB	cryst	384.95	193.60	142.83
8CB	opt	429.53	222.00	165.18
Dimer				
$\frac{1}{2}(8CB)_2$	cryst	368.43	193.21	145.42
$\frac{1}{2}(8CB)_2$	opt	412.58	214.37	176.65

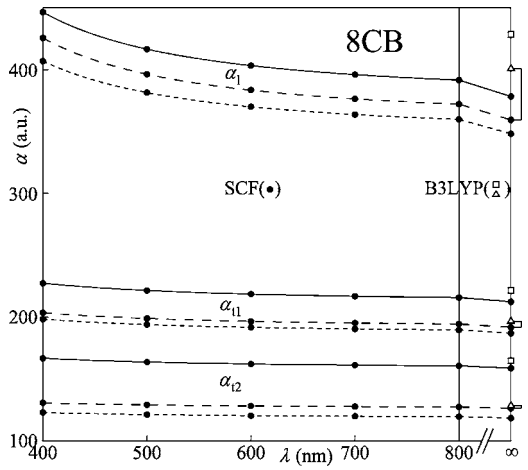

FIG. 15. Polarizabilities $\alpha_i(i=l,t_1,t_2)$ of 8CB in a.u. calculated for different basis sets (•—•: 4-31Gex, •---•: 6-31G*, •---•: 4-31G) as a function of wavelength λ. The frequency dependent polarizabilities (•) are calculated with the RPA-HF (SCF) method, the static polarizabilities, additionally with TD-DFT (B3LYP) (□: 6-31++G*, and △: 6-31G*).

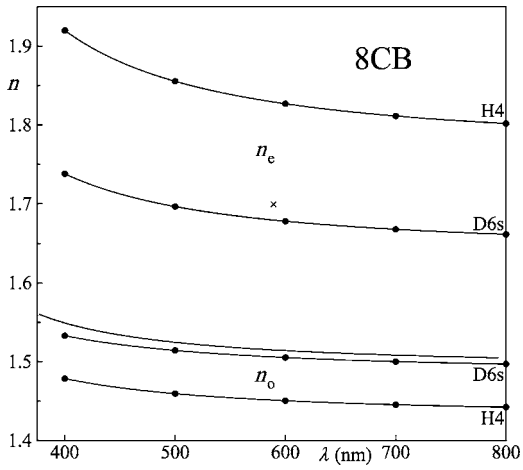

FIG. 16. Measured and calculated indices of refraction of 8CB as a function of wavelength λ. — and ×: measurement at 17.85 °C, H4: calculated with the Vuks-equations [see Eq. (12), assumption of a crystalline solid with $S=1$] (RPA-HF/4-31Gex), D6s: (RPA-HF/4-31Gex) values scaled by (B3LYP/6-31++G*) values and use of Eqs. (13) and (14) with $S=0.7$. In the calculation the density 0.9994 g/cm^3 [39] was used.

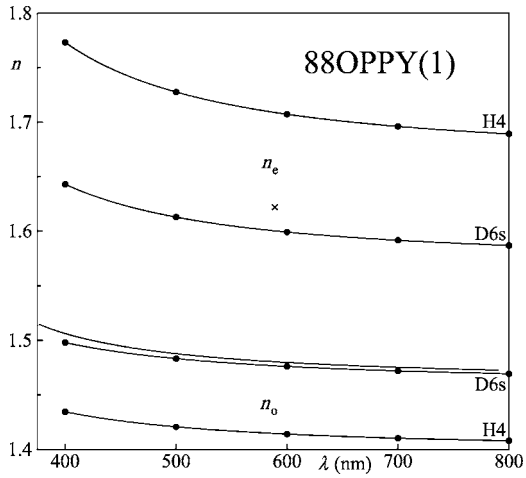

FIG. 17. Measured and calculated indices of refraction of 88OPPY(1) as a function of wavelength λ. — and ×: measurement at 56.72 °C, H4: calculated with the Vuks-equations [see Eq. (12), assumption of a crystalline solid with $S=1$] (RPA-HF/4-31Gex), D6s: (RPA-HF/4-31Gex) values scaled by (B3LYP/6-31++G*) values and use of Eqs. (13) and (14) with $S=0.7$. In the calculation the density 0.9646 g/cm^3 [40] was used.

see that by taking into account the influence of the order parameter (i.e., $S \neq 1$: not optimal orientation) the results for n_o deviate from the experimental results by 0.01 to 0.02, whereas the difference in n_e is slightly larger.

Finally, we can state a very good agreement between measurement and calculation. It is known that DFT-B3LYP is slightly overestimating polarizabilities when the basis set limit is approached: this we cannot afford within our calculations. Ruud *et al.* [42] have shown in their investigations for C_{60} that predicting the dispersion of the polarizabilities with the combination RPA-HF/6-31++G* leads to quite accurate results not far from experiment.

But because we do not really know the correct value of the order parameter there will always be a discrepancy between theory and experiment. If we would use $S=0.8$ for 8CB the agreement with experiment would be nearly perfect.

In order to get an idea about the quality of our calculations for the polarizabilities of the liquid crystal molecules we investigated in more detail three different molecular fragments: benzene, biphenyl, and *n*-octane. Our results are presented in Appendix C.

IV. SUMMARY

The dispersion of the ordinary index of refraction was measured for a series of smectic liquid crystals which are often used in free standing film experiments. Most of these liquid crystals show Sm-*A* phases, some show additional Sm-*C* phases. In the Sm-*C* phases two indices with the polarization direction parallel and perpendicular to the tilt direction can be measured.

The indices of refraction are measured by recording interference spectra in reflection from free standing smectic films. These films show in the Sm-*A* phase a perfect alignment of the director normal to the film surface. A drawback of the technique with free standing films is that only ordinary indices of refraction can be measured using normally incident light. An extension of the method of measurement would use oblique rays for the experiment. This allows us to determine the ordinary and the extraordinary indices of refraction.

The indices of refraction are measured for the accessible temperature range of the Sm-*A* phases. The results are presented by a modified Hartmann equation [see Eq. (A1)], the coefficients of which are given in Table V.

The data presented in this work had not been available up to now for smectic liquid crystals used for free standing film experiments. They are an important resource for the determination of films thicknesses with the interference technique.

Quantum chemical calculations for static and frequency dependent polarizabilities have been performed. With the help of the de Jeu-Bordewijk expression [Eqs. (13) and (14)] refractive indices have been calculated leading to a good agreement with our experimental data.

In the case of 8CB we compared monomer and dimer structures, i.e., parallel and antiparallel arrangements in the macroscopic ensemble, where the dimer has a bit smaller average polarizability compared to two monomers. The agreement between theory, using the phenomenological expression of de Jeu and Bordewijk [34,35], and our measurements is already so close that it is difficult to make a clear cut analysis of the contributions of the surrounding molecules. From the above analysis we cannot conclude that the type of arrangement (parallel versus antiparallel) has a significant influence on the refractive index.

What is left is a fully dynamical simulation of an ensemble of molecules to find out the order parameter *S*, which to our knowledge contributes most to the deviations from experiment. Already for benzene it is difficult to calculate absolutely accurate data for the polarizabilities without taking approximations (missing electron correlation, too small basis sets) and error cancellations (DFT) into account. Even experimental values for the anisotropies of α still differ by a

few percent, whereas average polarizabilities do not deviate too much between different experiments. If we compare the individual refractive indices n_o and n_e with experiment, we do need a correct description of the individual contributions to the principal values of the polarizabilities and we need in addition the correct magnitude of the order parameter in the smectic phase.

Temperature effects in α and n are taken into account by using the experimental values for the known density. Individual contributions from atomic motion, i.e., vibrational and rotational motion in/of the molecules, and inclusion of different conformations will lead to a further refinement in the frame of an *ab initio* molecular dynamics calculation, but seems to be now not necessary for the purpose of the present investigations.

In addition, investigations of molecular fragments (i.e., benzene, biphenyl, and octane) have been performed. They support our assumption (confirmed by other works in the literature [12,42]) that the prediction of polarizabilities and refractive indices by using RPA-HF and TD-DFT methods with reasonable flexible basis sets (4-31G* or 6-31++G*) will lead to useful support of experimental data.

ACKNOWLEDGMENTS

The authors thank Professor Staemmler for fruitful discussions. Financial support by the Deutsche Forschungsgemeinschaft is gratefully appreciated. The authors are much indebted to Professor Heppke, the Halle group, and the Merck KGaA for supplying the liquid crystals shown in Table I and Professor Mormann (Siegen) for the DSC spectra of the liquid crystals. The computations have been performed on the AMD-64-Opteron Cluster (HRZ, Siegen), the IBM-SP2 (SSC, Karlsruhe), and the Cray-SV1 (NIC, Jülich). The authors thank the computer centers for computer time.

APPENDIX A: NUMERICAL VALUES OF THE REFRACTIVE INDICES

The refractive indices were fitted with the function

$$n = A + BT + C/(D - T)^{0.2} + (E + FT + GT^2)/(\Lambda - H) \quad \text{(A1)}$$

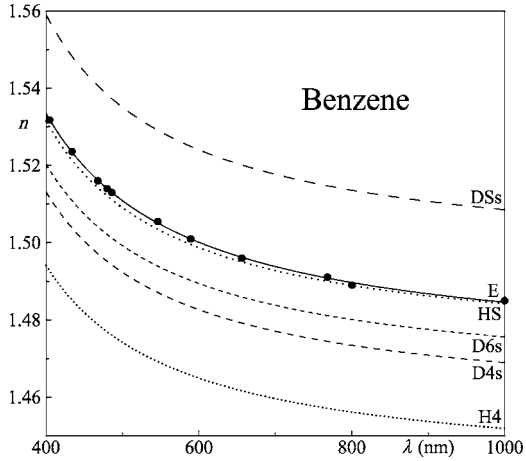

FIG. 18. Measured and calculated indices of refraction of benzene as a function of wavelength λ. HS: RPA(Sadlej), H4: RPA(4-31Gex), DSs: scaled from RPA(Sadlej) to B3LYP(Sadlej), D4s: scaled from RPA(4-31Gex) to B3LYP(4-31Gex), D6s: scaled from RPA(4-31Gex) to B3LYP(6-31++G*), and E: experiment (Samoc [60]).

with

$$T = (t - 30\,^\circ\text{C})/(30\,^\circ\text{C}); \quad \Lambda = \lambda/600\ \text{nm}. \quad \text{(A2)}$$

The first two terms of Eq. (A1) describe the linear dependence of the index of refraction on temperature. The third term is a Haller type [43] correction in the vicinity of the clearing point. The fourth term describes the dispersion with the Hartmann equation containing a temperature dependent-numerator. The coefficients are given in Table V. The deviations of the fitted refractive indices from the measured values are usually smaller than 0.0002 and grow sometimes at the short or long wavelengths end of the dispersion curve up to 0.0004.

APPENDIX B: QUANTUM CHEMICAL METHODS AND BASIS SETS

Theoretical investigations of the properties of "liquid crystal molecules" have been performed by using the program packages GAUSSIAN 98 (G98) [44] and GAUSSIAN 03

TABLE V. Coefficients for Eq. (A1). Temperature range from t_{min} to t_{max} in °C, range of wavelengths from 375 to 790 nm.

	$A\times10^4$	$B\times10^4$	$C\times10^4$	$D\times10^4$	$E\times10^4$	$F\times10^4$	$G\times10^4$	$H\times10^4$	t_{min}	t_{max}
8CB	14806.6	−72.7488	40.8644	1184.51	157.072	27.3045	29.0003	4194.27	17.9	32.0
9CB	14780.6	−66.4657	28.5697	5907.15	144.201	−1.58374	28.3771	4189.40	35.8	46.8
12CB	14610.5	−118.289	155.930	12707.0	136.700	−2.29374	8.63894	4092.37	41.8	57.3
8OCBP	14784.1	−59.9810	23.7783	12482.7	141.480	−17.7850	18.2462	4467.14	52.8	66.0
NPOB	14733.5	−63.8300	72.9431	12378.6	176.051	−79.4325	55.3680	4300.78	50.8	60.2
86OPPY	14562.9	−162.665	143.470	11367.8	132.444	−34.8643	30.7780	4119.24	47.7	56.9
88OPPY	14553.7	−223.370	203.450	13566.7	126.633	−29.7638	25.4237	4098.14	56.7	62.2
8OS5	14818.3	−83.7270	2.93683	10800.0	138.090	−8.97180	9.94000	4056.58	55.7	62.0
IS1401	14690.2	−90.6400	−4.52830	19155.9	101.990	−2.50880	0.17391	3623.59	34.7	108.2
IS1405	14713.3	−90.6724	31.5480	14832.7	126.959	−1.15091	2.49185	384.174	30.8	71.9

TABLE VI. Benzene, biphenyl, and *n*-octane: Static polarizabilities in a.u. calculated with Hartree-Fock (RPA-HF), DFT(B3LYP), and MP2 using different basis sets.

Methods	RPA-HF			B3LYP			MP2	Experiment
Basis sets	4-31Gex	6-31++G*	Sadlej	4-31Gex	6-31++G*	Sadlej	4-31Gex	
Molecules								
Benzene								
$\alpha_{uu}=\alpha_{vv}$	76.29	75.33	78.21	78.85	78.48	82.72	77.94	79.2 [16]
α_{ww}	37.27	41.38	44.98	38.32	41.46	44.50	39.02	47.7 [14]
Biphenyl								
α_{uu}	188.05	189.98	197.12	202.55	206.05	212.75		
α_{vv}	130.28	130.85	135.20	134.37	135.54	140.16		
α_{ww}	77.53	81.74	86.65	79.11	82.67	86.94		
n-Octane								
α_{uu}	110.42	108.24	121.13	118.80	119.54	132.38		
α_{vv}	85.65	84.66	89.68	90.88	90.78	96.20		
α_{ww}	80.93	80.88	84.20	85.14	84.75	89.07		

(G03) [45], DALTON [46], and TURBOMOLE [47]. For the optimizations of the structures a density functional method (DFT, G98) with the B3LYP functional has been used; the calculations are performed with all electron basis sets where split valence double zeta plus polarization functions (6-31G*) have been used. B3LYP is Becke's 3 parameter functional [48] with different exchange contributions (Slater, HF, Becke), the correlation functional of Vosko, Wilk, and Nusair [49] (functional III of VWN), and the nonlocal correlation provided by Lee, Yang, and Parr (LYP) [50]. Our choice for using B3LYP results from the experience of producing good structures with much less CPU time compared to the so-called high-level *ab initio* methods (e.g., coupled cluster).

Based on the optimized geometries, static and dynamic polarizabilities [51] have been calculated using (a) time-dependent Hartree-Fock (TD-HF) and (b) time-dependent DFT (TD-DFT) [(a) TD-HF: random phase approximation (RPA) with the integral-direct and parallel version [52] of the linear response theory [11] as implemented in the DALTON quantum chemistry program [46]: 16 processors, IBM-SP2 (SSC-Karlsruhe); (b) TD-DFT: program suite TURBOMOLE [47] (parallel version: NIC-Jülich and HRZ-Siegen)].

The choice of the basis set for calculating polarizabilities is crucial. Accurate RPA values have been obtained using a 4-31G basis set [53,54] with additional polarizing and diffuse p(C:0.05)- and d(C:0.05)-functions on the heavier elements, i.e., C, N, O, etc. (in the present work called

TABLE VII. Benzene: Frequency dependent polarizabilities in a.u. calculated with random phase approximation (RPA-HF) and TD-DFT (B3LYP) using different basis sets.

Methods		RPA-HF[a]	RPA-HF[a]	TD-B3LYP[b]	TD-B3LYP[c]
Basis sets		4-31Gex	Sadlej	6-31++G*	Sadlej
λ (nm)					
400	α_{uu}	83.94	86.40	87.70	92.25
	α_{ww}	39.74	47.96	44.76	47.54
500		80.91	83.14	84.02	88.41
		38.79	46.81	43.49	46.35
600		79.40	81.52	82.22	86.55
		38.30	46.22	42.85	45.75
700		78.54	80.60	81.20	85.47
		38.02	45.88	42.48	45.41
800		77.99	80.02	80.55	84.80
		37.84	45.67	42.25	45.19
∞		76.29	78.21	78.56	82.72
		37.27	44.98	41.52	44.50

[a]RPA-HF: random phase approximation; response theory in DALTON [46].
[b]B3LYP in TURBOMOLE [47].
[c]B3LYP in G98 [45].

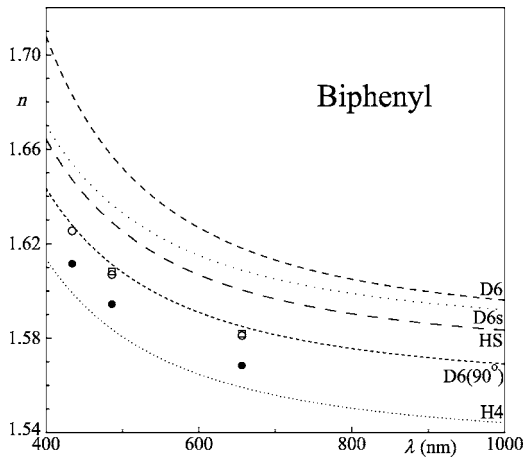

FIG. 19. Measured and calculated indices of refraction of biphenyl as a function of wavelength (density 0.9717 g/cm^3 at 99 °C [62]). HS: RPA(Sadlej), H4: RPA(4-31Gex), D6s: scaled from RPA(4-31Gex) to B3LYP(6-31++G*), D6: B3LYP(6-31++G*), D6[90(○)]: B3LYP(6-31++G*) (torsion angle 90°), and experimental values at 99 (●), 77 (○), and 73 °C (□).

4-31Gex). The quality of RPA with this basis set has been described in an earlier study by Norman *et al.* [55] for the polarizabilities and hyperpolarizabilities of a series of polyacene molecules. The results for benzene have been reported to be within 2% of the results for the largest basis set, close to the HF limit [56]. This tailored basis set has been tested for optical molecular properties in several previous studies (e.g., C_{60}: [42,57]; smaller organic molecules: Refs. 28–30 in Ref. [57]).

APPENDIX C: POLARIZABILITIES AND REFRACTIVE INDICES OF BENZENE, BIPHENYL, AND *n*-OCTANE

There are a lot of experimental [14,58] and theoretical [59] results available for the polarizability of benzene. Our results presented in Tables VI (static polarizabilities) and VII (frequency dependent polarizabilities), using the same methods (in addition MP2) and basis sets, including the even more flexible basis set of Sadlej [30], are in agreement with other theoretical investigations in the literature [59].

The refractive indices (see Fig. 18) were calculated with Eq. (11). They show similar dispersion behavior for RPA-HF and TD-DFT. The calculated dispersion is nearly in perfect agreement with experiment [60]. D6s (B3LYP/6-31++G* scaled from RPA/4-31Gex) was the "best" choice for the liquid crystal molecules and the curve lies a bit below the experimental one; the Sadlej basis set is overestimating and 4-31G* is a bit underestimating. The frequency dependence is better reproduced by using RPA-HF; TD-DFT is increasing a bit too fast towards lower wavelengths (see for comparison: RPA-HF/Sadlej and TD-DFT/Sadlej in Table VII).

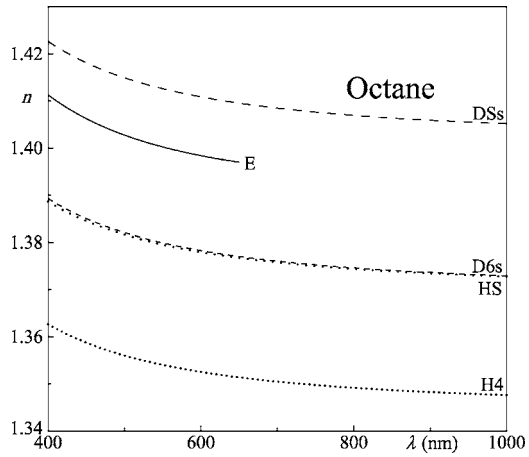

FIG. 20. Measured and calculated indices of refraction of *n*-octane as a function of wavelength (density 0.7028 g/cm^3 at 20 °C [65]). H4: RPA(4-31Gex), HS: RPA(Sadlej), D6s: scaled from RPA(4-31Gex) to B3LYP(6-31++G*), DSs: scaled from RPA(4-31Gex) to B3LYP(Sadlej), and E: fit to the experimental values at 20 °C up to 650 nm [66].

TABLE VIII. Biphenyl and *n*-octane: Frequency dependent polarizabilities in a.u. calculated with random phase approximation (RPA-HF) and TD-DFT (B3LYP) using different basis sets.

Molecules		Biphenyl (≈39°)				Biphenyl (90°)	*n*-octane	
Methods		RPA-HF[a]	RPA-HF[a]	TD-B3LYP[b]	TD-B3LYP[b]	TD-B3LYP[b]	RPA-HF[a]	RPA- HF[a]
Basis sets		4-31Gex	Sadlej	6-31++G*	Sadlej	6-31++G*	4-31Gex	Sadlej
λ (nm)								
400	α_{uu}	218.79	232.23	256.72	265.28	216.69	115.87	126.92
	α_{vv}	142.29	148.00	150.67	155.54	122.17	89.53	93.60
	α_{ww}	82.75	92.47	89.37	93.40	121.99	84.39	87.74
500		205.85	217.20	233.89	241.43	204.99	113.84	124.76
		137.54	142.90	144.59	149.30	117.76	88.08	92.14
		80.72	90.19	86.78	90.89	117.59	83.10	86.42
600		199.82	210.33	224.14	231.31	199.41	112.77	123.62
		135.18	140.39	141.65	146.29	115.60	87.32	91.37
		79.70	89.05	85.49	89.64	115.43	82.42	85.72
700		196.46	206.53	218.91	225.89	196.26	112.14	122.95
		133.82	138.94	139.98	144.59	114.36	86.87	90.91
		79.10	88.39	84.75	88.93	114.20	82.02	85.31
800		194.38	204.19	215.73	222.61	194.30	111.73	122.52
		132.96	138.03	138.94	143.52	112.69	86.58	90.62
		78.73	87.97	84.29	88.48	113.42	81.76	85.05
∞		188.04	197.12	206.37	212.96	188.29	110.42	121.13
		130.28	135.20	135.72	140.23	111.17	85.65	89.68
		77.53	86.65	82.83	87.06	111.02	80.93	84.20

[a]RPA-HF: random phase approximation; response theory in DALTON [46].
[b]B3LYP in TURBOMOLE [47].

Samoc [60] performed in addition to experimental refractive index investigations semiempirical coupled perturbed Hartree-Fock calculations using MOPAC 93 [61] and the AM1-method: the theoretical and experimental dispersion curves are shifted with respect to each other and the slopes depart in the region of strong dispersion, where electronic resonances are approached.

Similar results are presented for biphenyl (for polarizabilities see Tables VI and VIII). Here the situation is a bit more complicated because refractive index data in the liquid isotropic phase are only available at higher temperatures (Fig. 19): 73, 79, and 99 °C [62–64]. In this case the rotation of the two phenyl groups to each other has to be taken into account [the barrier height for torsion is 10.5 kJ/mol (B3LYP/6-31G*)], which leads to a reduction of the polarizability and the refractive index. In Fig. 19 the refractive index is plotted for the optimized structure with a torsion angle of ≈39° and for the structure with a torsion angle of 90°. The calculated values for the refractive index are even with torsion angle 90° still a bit larger then the experimental data. In addition, it is known that TD-DFT-B3LYP/6-31++G* slightly overestimates the refractive index. Finally we can say that the dispersion behavior is in good agreement with the experiment.

In the case of *n*-octane (see Tables VI and VIII and Fig. 20) the dispersion behavior of the refractive index agrees with the experiment up to 650 nm, the longest wavelength for which the refractive indices were measured by Kerl and Varchim [66].

[1] S. Elston and R. Sambles, *The Optics of Thermotropic Liquid Crystals* (Taylor and Francis, London, 1998).
[2] G. Pelzl, in *Handbook of Liquid Crystals* (Wiley-VCH, Weinheim, 1998), Vol. 2A, Chap. 2.4, p. 128.
[3] M. Warenghem and C. P. Grover, Rev. Phys. Appl. **23**, 1169 (1988).
[4] M. Warenghem and G. Joly, Mol. Cryst. Liq. Cryst. **207**, 205 (1991).
[5] C. McBride, M. R. Wilson, and J. A. K. Howard, Mol. Phys. **93**, 955 (1998).
[6] M. P. Allen, M. A. Warren, and M. R. Wilson, Phys. Rev. E **57**, 5585 (1998).
[7] T. Helgaker, P. Jørgensen, and J. Olsen, *Molecular Electronic-Structure Theory* (Wiley-VCH, Weinheim, 2000).
[8] F. Jensen, *Introduction to Computational Chemistry* (Wiley-VCH, Weinheim, 1999).
[9] S. P. A. Sauer, *The ab initio Calculation of Molecular Properties* (Lec. Notes for the 3. MERCOSUR School on Molecular Physics, 2001).
[10] G. C. Schatz and M. A. Ratner, *Quantum Mechanics in Chemistry* (Prentice-Hall, Engelwood Cliffs, NJ, 1993).
[11] J. Olsen and P. Jørgensen, J. Chem. Phys. **82**, 3235 (1985).
[12] C. van Caillie and R. D. Amos, Chem. Phys. Lett. **328**, 446 (2000).
[13] T. B. Pedersen, A. M. J. S. de Meras, and H. Koch, J. Chem. Phys. **120**, 8887 (2004).
[14] M. Okruss, R. Müller, and A. Hese, J. Chem. Phys. **110**, 10393 (1999).
[15] A. Protiere and M. Camail, Mol. Phys. **29**, 1473 (1975).
[16] R. J. Alms, A. K. Burham, and W. H. Flygare, J. Chem. Phys. **63**, 3221 (1975).
[17] R. Antoine, P. Dugourd, D. Rayane, E. Benichou, M. Broyer, F. Chandezon, and C. Gurt, J. Chem. Phys. **110**, 9771 (1999).
[18] A. Ballard, K. Bonin, and J. Louderback, J. Chem. Phys. **113**, 5732 (2000).
[19] W. Nebe, Feingerätetechnik **20**, 554 (1971).
[20] R. Jaquet and F. Schneider, Phys. Rev. E **67**, 021707 (2003).
[21] H. Kelker and R. Hatz, *Handbook of Liquid Crystals* (Verlag Chemie, Weinheim, Germany, 1980), p. 257.
[22] C. David and D. Baeyens-Volant, Mol. Cryst. Liq. Cryst. **59**, 181 (1980).
[23] T. E. Lockhart, D. W. Allender, E. Gelerinter, and D. L. Johnson, Phys. Rev. A **20**, 1655 (1979).
[24] T. E. Lockhart, E. Gelerinter, and M. E. Neubert, Phys. Rev. A **25**, 2262 (1982).
[25] M. Koden and T. Anabuki, Ferroelectrics **121**, 295 (1991).
[26] E. K. Dalskov and S. P. A. Sauer, J. Phys. Chem. A **102**, 5269 (1998).
[27] S.-L. L. Y.-J. Lu, Chem. Phys. **179**, 431 (1994).
[28] G. B. Talapatra, N. Manickam, M. Samoc, M. E. Orcyc, S. P. Karna, and P. N. Prasad, J. Phys. Chem. **96**, 5206 (1992).
[29] N. Matsuzawa and D. A. Dixon, J. Phys. Chem. **96**, 6872 (1992).
[30] A. J. Sadlej, Collect. Czech. Chem. Commun. **53**, 1995 (1995).
[31] J. R. Partington, *An Advanced Treatese on Physical Chemistry. Physico Chemical Optics*, Vol. 4 (Longmans, Green and Co., London, 1967).
[32] C. J. F. Böttcher and P. Bordewijk, *Theory of Electric Polarization*, Vol. 2, 2nd ed. (Elsevier, Amsterdam, 1978).
[33] M. F. Vuks, Opt. Spektrosk. **20**, 644 (1966).
[34] W. H. de Jeu and P. Bordewijk, J. Chem. Phys. **68**, 109 (1978).
[35] W. H. de Jeu, *Physical Properties of Liquid Crystalline Materials* (Gordon and Breach, New York, 1980).
[36] A. J. Leadbetter, R. M. Richardson, and C. N. Colling, J. Phys. (Paris) **36**, C1 (1975).
[37] *Molecular Orbital Package MOS-F V4.2* (J. J. P. Stewart and Fujitsu Limited, Tokyo, 1999).
[38] M. Kuribayashi and K. Hori, Acta Crystallogr., Sect. C: Cryst. Struct. Commun. **C54**, 1475 (1998).
[39] H. Kneppe and F. Schneider (unpublished results).
[40] R. Kiefer and G. Baur, Liq. Cryst. **7**, 815 (1990).
[41] R. G. Horn, J. Phys. (Paris) **39**, 105 (1978); P. L. Sherell and D. A. Crellin, *ibid.* **40**, C3–211 (1979); M. Constant and D. Decoster, J. Chem. Phys. **76**, 1708 (1982); B. M. Fung, C.-D. Poon, M. Gangoda, E. L. Enwall, T. A. D. Dip, and C. V. Bui, Mol. Cryst. Liq. Cryst. **141**, 267 (1986); T. Kobayashi, H. Yoshida, A. D. L. Chandani, S. Kobinata, and S. Maeda, *ibid.* **136**, 267 (1986).
[42] K. Ruud, D. Jonsson, and P. Taylor, J. Chem. Phys. **114**, 4331

(2001).
[43] I. Haller, Prog. Solid State Chem. **10**, 103 (1975).
[44] M. J. Frisch *et al.*, *Gaussian 98* (Gaussian, Inc., Pittsburgh PA, 1998).
[45] M. J. Frisch *et al.*, *Gaussian 03* (Gaussian, Inc., Pittsburgh, PA, 2003).
[46] T. Helgaker, H. J. A. Jensen, P. Jørgensen *et al.*, *Dalton, an ab initio Electronic Structure Program, Release 1.2* (2001).
[47] R. Ahlrichs, M. Bär, M. Häser, H. Horn, and C. Kölmel, Chem. Phys. Lett. **162**, 165 (1989).
[48] A. D. Becke, J. Chem. Phys. **98**, 5648 (1993).
[49] S. H. Vosko, L. Wilk, and M. Nusair, Can. J. Phys. **58**, 1200 (1980).
[50] C. Lee, W. Yang, and R. G. Parr, Phys. Rev. B **37**, 785 (1988).
[51] P. Lazzeretti, Adv. Chem. Phys. **75**, 507 (1989).
[52] K. Ruud, H. Ågren, T. Helgaker *et al.*, Chem. Phys. Lett. **285**, 205 (1998).
[53] W. J. Hehre and W. A. Lathan, J. Chem. Phys. **56**, 5255 (1972).
[54] R. Ditchfield, W. J. Hehre, and J. A. Pople, J. Chem. Phys. **54**, 724 (1971).
[55] P. Norman, D. Jonsson, H. Ågren, P. Dahle, K. Ruud, T. Helgaker, and H. Koch, Chem. Phys. Lett. **253**, 1 (1996).
[56] P. Lazzeretti, M. Malagoli, and R. Zanasi, Chem. Phys. Lett. **167**, 101 (1990).
[57] P. Norman, Y. Luo, D. Jonsson, and H. Ågren, J. Chem. Phys. **106**, 8788 (1997).
[58] Refs. [9–11,20–22] in Ref. [14].
[59] Refs. [3–7,9,23] in Ref. [14].
[60] A. Samoc, J. Appl. Phys. **94**, 6167 (2003).
[61] *Molecular Orbital Package, version 93* (J. J. P. Stewart and Fujitsu Limited, Tokyo, 1993).
[62] W. H. Perkin, J. Chem. Soc. **69**, 1025 (1896).
[63] M. J. F. Eijkman, Recl. Trav. Chim. Pays-Bas **12**, 157 (1893).
[64] K. v. Auwers and A. Frühling, Justus Liebigs Ann. Chem. **422**, 192 (1921).
[65] S. Budavari, M. J. O'Neil, A. Smith, and P. E. Heckelman, *The Merck Index* (Merck & Co., Inc., Rahway, NJ, 1989).
[66] K. Kerl and H. Varchmin, J. Mol. Struct. **349**, 257 (1995).